Study of internal structures of $^{9,\,10}$Be and $^{10}$B in scattering of $^{4}$He from $^{9}$Be



2014 J. Phys. G: Nucl. Part. Phys. 41 035102

(http://iopscience.iop.org/0954-3899/41/3/035102)

IOP Publishing Journal of Physics G: Nuclear and Particle Physics

J. Phys. G: Nucl. Part. Phys. **41** (2014) 035102 (14pp) doi:10.1088/0954-3899/41/3/035102

# Study of internal structures of $^{9,10}$Be and $^{10}$B in scattering of $^{4}$He from $^{9}$Be

**S M Lukyanov[1], A S Denikin[1,2], E I Voskoboynik[1], S V Khlebnikov[3,4], M N Harakeh[5,6], V A Maslov[1], Yu E Penionzhkevich[1,7], Yu G Sobolev[1], W H Trzaska[3], G P Tyurin[3] and K A Kuterbekov[8]**

[1] Flerov Laboratory of Nuclear Reactions, Dubna, Russia
[2] Dubna International University, Dubna, Russia
[3] Department of Physics, University of Jyväskylä, Jyväskylä, Finland
[4] Khlopin Institute, St. Petersburg, Russia
[5] Kernfysisch Versneller Instituut, University of Groningen, Groningen, The Netherlands
[6] GANIL, CEA/DSM-CNRS/IN2P3, F-14076 Caen, France
[7] National Research Nuclear University MEPhI, Moscow, Russia
[8] Eurasian Gumilev University, Astana, Kazakhstan

E-mail: lukyan@nrmail.jinr.ru

Received 14 October 2013, revised 10 December 2013
Accepted for publication 20 December 2013
Published 5 February 2014

**Abstract**

A study of inelastic scattering and single-particle transfer reactions was performed using a 63 MeV alpha beam on a $^{9}$Be target. Angular distributions of the differential cross sections for the $^{9}$Be($\alpha$,$\alpha'$)$^{9}$Be$^{*}$, $^{9}$Be($\alpha$, $^{3}$He)$^{10}$Be and $^{9}$Be($\alpha$,$t$)$^{10}$B reactions were measured. Experimental angular distributions of the differential cross sections for the ground states and a few low-lying states in the final nuclei were analyzed in the framework of the optical model, coupled channels and distorted-wave Born approximation. An analysis of the obtained spectroscopic factors was performed.

Keywords: inelatic scattering, angular distribution, differential cross section, optical model, DWBA

## 1. Introduction

In recent years, the study of light, weakly-bound nuclei [1, 2] has intensified due to the significant progress made with radioactive beam facilities. It has led to a resurgence of interest in the study of light stable nuclei such as $^{6,7}$Li and $^{9}$Be. It has been shown that in light nuclei the nucleons tend to group into clusters, relative motion of which defines to a large extent of

the properties of these nuclei. Consequently, the cluster structures of their ground as well as low-lying excited states have been in the focus of studies. As examples, the nuclei $^{6}$Li and $^{7}$Li are both well described by two-body cluster models ($\alpha$ + and $\alpha$ + t, respectively). Another interesting nuclide is $^{9}$Be, which could be described as an $\alpha + \alpha +$ n three-body configuration; one may also consider it as a nuclear system with two-body configurations: $^{8}$Be + n or $^{5}$He + $\alpha$.

The addition of a second valence neutron to $^{9}$Be leads to another intriguing nucleus, $^{10}$Be. A microscopic $\alpha + \alpha +$ n + n cluster model was proposed for $^{10}$Be in order to clarify the relation between the configurations of the valence neutrons and the $\alpha + \alpha$ core.

Recently, special attention has been focused on the role of the extra 'valence' [3] nucleons, and their influence on the cluster structure of the excited states. A semi-quantitative discussion of this subject can be found in [3], where the two-center molecular states in $^{9}$B, $^{9}$Be, $^{10}$Be and $^{10}$B nuclei were considered in the framework of a molecular-type model.

One of the tools to study nuclear structure is scattering of a projectile, such as $^{3,4}$He, from a target nucleus, the structure of which is going to be studied. This method is based on angular-distribution measurements of elastic and inelastic scattering of transfer-reaction projectile-like products. The energy spectra of these products bear information about the internal structure of the incoming and outgoing nuclei.

Alpha scattering from a $^{9}$Be target was measured at a bombarding energy $E_{\alpha} = 65$ MeV for the first time by Harakeh *et al* [4] and later by Roy *et al* [5]. Optical model (OM) analysis of the elastic scattering data was performed, and distorted-wave Born approximation (DWBA) and coupled-channel (CC) calculations were also done for inelastic scattering and single-particle transfer channels. A molecular-type rotational band was used to describe the data.

The data of [6] demonstrated the measurement in inverse kinematics of a 65 MeV $^{12}$C beam scattered from a $^{9}$Be target. The experimental data were analyzed in [7]. The calculations agree well with data for elastic scattering and excitation of the $5/2^{-}$ resonance of $^{9}$Be at 2.43 MeV, while data for the $1/2^{+}$ (1.68 MeV) state excitation were not well described by their model. This was as expected from structure calculations of $^{9}$Be treating this state as almost pure $^{8}$Be + n cluster configuration. A rather different conclusion was drawn in [8]. It was found that the decay branch n + $^{8}$Be($2^{+}$) provides a small fraction of the decay of the $5/2^{-}$ state. In total agreement with this finding, Charity *et al* [9] recently confirmed that decay of $^{9}$B has a dominant branch to $\alpha$ + $^{5}$Li implying that 'the corresponding mirror state in $^{9}$Be would be expected to decay through the mirror channel $\alpha$ + $^{5}$He, instead of through the n + $^{8}$Be($2^{+}$) channel'.

This article makes an attempt to shed light on the internal structure of $^{9,10}$Be and $^{10}$B nuclei by scattering of $^{4}$He ions from a $^{9}$Be target. We expected that the sensitivity of the high precision alpha scattering data to the internal structure of the studied nuclei could be demonstrated.

## 2. Experiment

The experiment was performed at the K130 Cyclotron facility of the Accelerator Laboratory of the Physics Department of Jyväskylä University. The beam energy of $^{4}$He ions was 63 MeV. The average beam current during the experiment was maintained at 3 nA. The self-supporting Be target was prepared from a 99% pure thin foil of beryllium. The target thickness was 7 $\mu$m. Peaks due to carbon and oxygen contaminations were not observed in the energy spectra.

To measure (in)-elastically scattered ions, two telescopes each consisting of Si-Si(Li) detectors with thicknesses of 100 $\mu$m and 3 mm, respectively, were used. Each pair of detectors

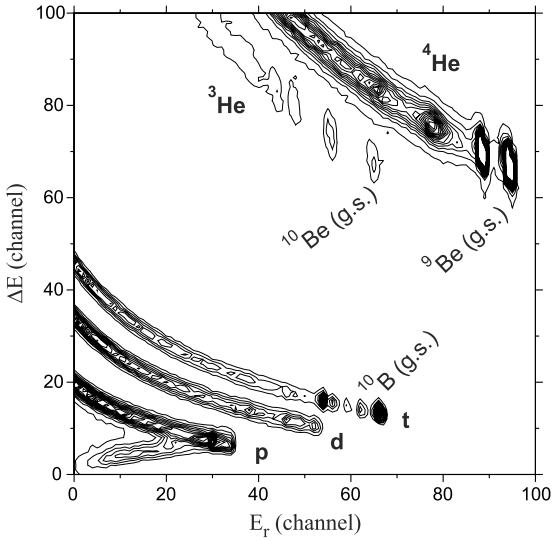


**Figure 1.** Reaction product yields versus measured energy loss ΔE and residual energy $E_r$ measured by the Si-Si(Li) telescope. The loci for $^{3,4}$He, p, d and t are clearly visible.

**Table 1.** Reaction channels and their Q- values.

| Reaction channel | Q-values (MeV) |
|---|---|
| $^9\mathrm{Be} + {}^4\mathrm{He} \rightarrow {}^{10}\mathrm{Be} + {}^3\mathrm{He}$ | −13.8 |
| $^9\mathrm{Be} + {}^4\mathrm{He} \rightarrow {}^{10}\mathrm{B} + \mathrm{t}$ | −13.2 |
| $^9\mathrm{Be} + {}^4\mathrm{He} \rightarrow {}^{11}\mathrm{B} + \mathrm{d}$ | −8.0 |
| $^9\mathrm{Be} + {}^4\mathrm{He} \rightarrow {}^{12}\mathrm{B} + \mathrm{p}$ | −6.9 |

was mounted at a distance of about 45 cm from the target. Particle identification was performed based on the energy-loss measurements of ΔE and residual energy $E_r$, i.e. the so-called ΔE-E method. The Si-telescopes were mounted on rotating supports, which allowed to obtain data from $\theta_{lab} = 20^\circ$ to $\theta_{lab} = 107^\circ$ in steps of 1°–2°.

The overall energy resolution of the telescopes was nearly 200 keV. An example of two-dimensional plot (yield versus energy loss ΔE and residual energy $E_r$, measured by Si-Si(Li) detectors) is shown in figure 1. Excellent energy resolutions of both ΔE and E detectors allowed identifying $^{3,4}$He, t, d and p unambiguously. These detected particles were produced in the reaction channels listed in table 1.

The reaction channel leading to the production of $^7\mathrm{Be} + {}^6\mathrm{He}$ has minimal probability due to the low Q-value. Other reaction channels take place at higher Q-values and consequently have larger cross sections, as it is shown in figure 1. The production yield of $^6$He starts to be visible only when plotting the $z$-axis (yield) in logarithmic scale; it is not shown in figure 1.

Comparing with the experimental technique of [5] we have the advantage to distinguish the particles p, d, t, $^3$He and $^4$He and determine their total deposited energies. The total energies were obtained after energy calibration of all Si-detectors and summing of energy signals of the ΔE and $E_r$ detectors. The spectra of total deposited energy are shown in figure 2 for t, $^3$He and $^4$He. All peaks, which can be observed in the histograms in figure 2, were identified and found to belong to the ground and excited states of $^9$Be, $^{10}$Be and $^{10}$B, as the complementary products to detected particles $^4$He, $^3$He, and t, respectively. We were not able to get information

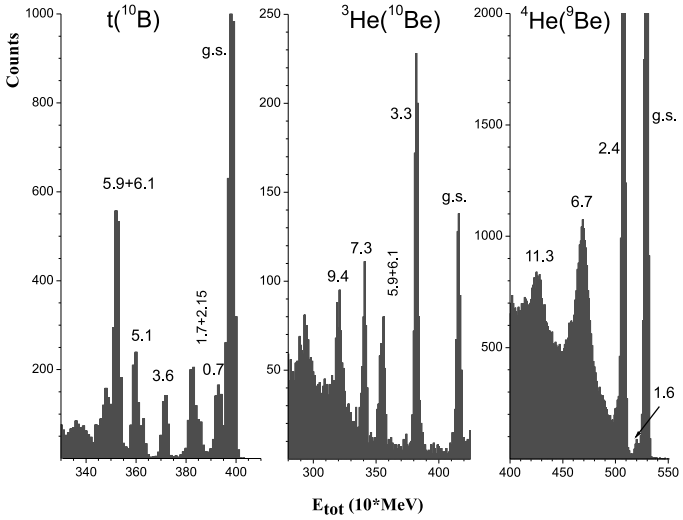


**Figure 2.** Measured spectra of total energies for $^{9}$Be($\alpha$,t)$^{10}$B (left), $^{9}$Be($\alpha$,$^{3}$He)$^{10}$Be (middle) and $^{9}$Be($\alpha$, $\alpha'$)$^{9}$Be (right) reaction channels. The ground and most of the populated excited states of $^{10}$B, $^{10}$Be and $^{9}$Be are unambiguously identified.

about states in $^{11,12}$B, due to the restricted thickness of the Si(Li) detectors, as a consequence of which protons and deutrons punched through and were not stopped in the Si(Li) detectors.

We found excellent agreement between excited states observed in our experiment with those previously measured for $^{9}$Be [4, 5, 10], $^{10}$Be [11], and $^{10}$B [12]. Because the incident beam energy was rather high (15.75 MeV/*u*), the observed states are most likely populated in one-step direct transfer reactions. Another advantage is that the two nuclei $^{10}$Be and $^{10}$B, belonging to A = 10 multiplet, are populated in the same reaction.

## 3. Results

### *3.1.* $^{9}$*Be*

Measured differential cross sections for the ground and low-lying excited states of $^{9}$Be are presented in figure 3. Due to low statistics we were not able to get the angular distribution for the first-excited $1/2^{+}$ state of $^{9}$Be at 1.6 MeV. The oscillations at small angles of the angular distributions for the ground state ($3/2^{-}$) and the first-excited state ($5/2^{-}$) are in anti-phase. No significant oscillatory structure was observed for the angular distributions of the $7/2^{-}$ and $9/2^{-}$ states.

Comparison with the results for the ground state of the previous measurements [4, 5] (open symbols) demonstrates a good agreement at small scattering angles. The disagreement is observed at angles larger than 70° where our data are smaller than those of [5]. From the technical point of view, this difference could be explained by absence of particle identification in [5] where Si(Li) detectors were used to measure the total energy only, without a $\Delta$E measurement that would allow Z and A identification of the detected particles. Another reason could also be due to a different method used for subtraction of the continuum under the peak. The same reasons are responsible for the difference between our data and those of [5] for the level at 2.43 MeV for angles large than 70°.

Figure 3 shows measured differential cross sections for the elastic and inelastic scattering (symbols) together with the results of theoretical calculations (curves) performed within OM

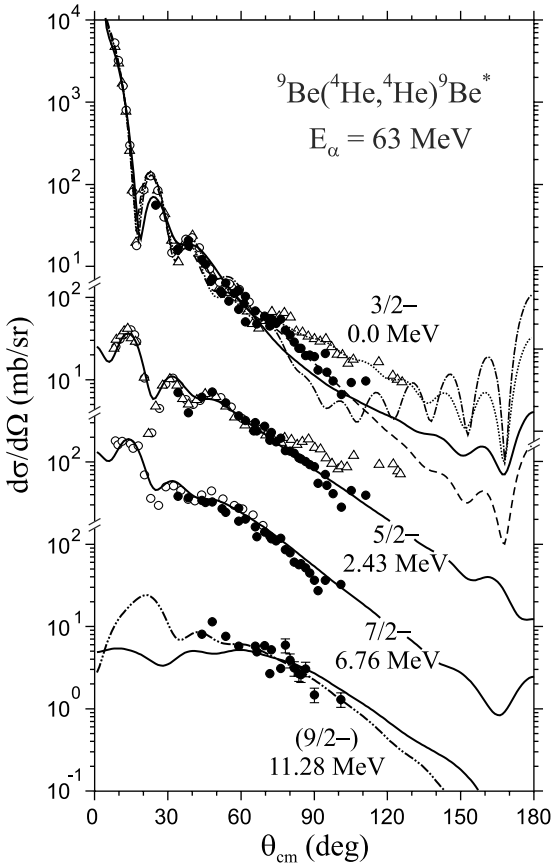


**Figure 3.** Differential cross sections for the $^4$He (63 MeV) + $^9$Be scattering reactions. Data obtained in the present work are shown by symbols •, data from [4, 5] are denoted by ○ and △ open symbols, respectively. Angular distributions of elastic and inelastic scattering to the $5/2^-$ (2.43 MeV), $7/2^-$ (6.76 MeV) and $9/2^-$ (11.28 MeV) $^9$Be states are shown. The curves represent the results of the optical-model and coupled-channel calculations (see explanation in text).

and CC approaches. Theoretical curves were obtained with the aid of NRV server OM routine [13] and the ECIS06 CC code [14, 15].

Firstly, let us consider the analysis of the elastic scattering cross section. The optical potential was chosen in the usual Woods–Saxon form

$$V(r) = -V_0 f(r, R_V, a_V) - \mathrm{i}W_0 f(r, R_W, a_W),$$

where the function $f(r, R, a) = (1 + \mathrm{e}^{(r-R)/a})^{-1}$. Potential parameters (OM1) fitted within the OM to the measured experimental data are listed in table 2. The corresponding curve is shown in figure 3 as a dashed line and demonstrates good agreement with the obtained data. In addition, the calculation of elastic scattering cross section was performed with the parameters (OM2), recommended in [4]. It is plotted as dash–dotted line in figure 3. One may see that OM2 parameters of [4] provide poorer agreement with the data at large angles since the OM2 parameters were obtained by fitting the data in a narrower angular range. The main differences between the OM1 and OM2 sets are the shallower depth of the real part and the larger diffuseness parameters of the potential found in this work.

**Table 2.** Potential parameters used within optical-model and coupled-channels approaches.

| | $V_0$(MeV) | $r_V$(fm) | $a_V$ (fm) | $W_0$(MeV) | $r_W$(fm) | $a_W$ (fm) | $r_C$(fm) |
|---|---|---|---|---|---|---|---|
| $\alpha + {}^{9}$Be (OM1) | 101.0 | 1.40 | 0.75 | 32.70 | 1.50 | 0.75 | 1.30 |
| $\alpha + {}^{9}$Be (CC) | 96.82 | 1.19 | 0.75 | 11.84 | 1.61 | 0.75 | 1.30 |
| $\alpha + {}^{9}$Be (OM2)[4] | 146.8 | 1.49 | 0.59 | 35.95 | 1.49 | 0.59 | 1.25 |
| $\alpha + {}^{9}$Be (OM3)[a] | 109.1 | 1.48 | 0.65 | 40.00 | 1.34 | 0.727 | 1.30 |
| ${}^{3}$He + ${}^{10}$Be[b] | 95.0 | 0.95 | 0.815 | 8.00 | 1.60 | 0.726 | 1.07 |
| ${}^{3}$H + ${}^{10}$B[c] | 95.0 | 1.04 | 0.815 | 3.00 | 1.867 | 0.47 | 1.07 |
| ${}^{3}$He or ${}^{3}$H + ${}^{10}$B [4] | 132.9 | 1.54 | 0.57 | 19.50 | 1.82 | 0.22 | 0.81 |

[a] Parameters are obtained by fitting the elastic scattering data of [5].
[b] Parameters were taken from [16]. Real and imaginary depths and radii were modified within 10–15% of magnitude in order to fit experimental data for neutron transfer to the ${}^{10}$Be ground state.
[c] The ${}^{3}$He + ${}^{10}$Be parameters (were taken from [16]) were used as initial set and then parameters were fitted to reproduce experimental data for proton transfer to the ${}^{10}$B ground state.

Our fitting (OM3) of the data [5] for the ground state of ${}^{9}$Be are also given in table 2. The corresponding angular distribution is shown in figure 3 by dotted line. The obtained parameters are rather close to the ones found in [5], except a noticeably smaller radius of the imaginary part. It results in the larger elastic scattering cross sections at large deflection angles.

The simplest view of the ${}^{9}$Be nucleus is that it is a strongly deformed three-body system consisting of two $\alpha$ particles held together by a weakly-bound neutron. It is very natural that different molecule-like states may appear in the excited states. It is the aim of research in this mass region to make a systematic study of structure changes with increasing excitation energy.

Due to the Borromean structure of ${}^{9}$Be, it will be configured as two alpha particles plus a neutron or as two unstable intermediate nuclei: (i) ${}^{8}$Be or (ii) ${}^{5}$He in combination with a neutron and an $\alpha$-particle, respectively. However, to distinguish break-up into ${}^{4}$He and ${}^{5}$He is not a trivial kinematical problem; nevertheless, some attempt has been successfully undertaken [17]. The structure of ${}^{9}$Be through ${}^{8}$Be + n has been quantified for the low-lying excited states in ${}^{9}$Be. Higher excited levels are associated with a ${}^{5}$He cluster. One of the aims of the present experiment was to study the peculiarity of the angular distributions of elastic and inelastic scattering, mainly $5/2^-$, $7/2^-$ and $9/2^-$ states, to try to learn something about their cluster structure.

Analysis of inelastic scattering data within the DWBA or CC approach allows to extract the information on the deformation of an excited nucleus treating these states as collective rotational excitations. The corresponding coupling matrix elements include, in addition to the radial form-factor, the deformation length $\beta_\lambda R_V$, where $\beta_\lambda$ is a deformation parameter, $\lambda$ is a multipolarity of the transition defined by the transferred angular momentum and $R_V = r_V A^{1/3}$ is an interaction radius depending on the mass A of the excited nucleus.

It is known [4, 5, 18–20] that ${}^{9}$Be has a rotational band ($K^\pi = 3/2^-$) built on its ground state. In previous studies only ground and excited states of the band were analyzed together in the CC framework. One may expect [21, 22] that all angular distributions shown in figure 3 are related to the same rotational band. So far, the values of spin and parity of the 11.28 MeV state were uncertain. No direct measurements were done. This level was listed either $7/2^-$ or $9/2^-$ state in the literature and databases. Following [19], we consider this state to belong to the rotational band and therefore to have spin-parity $9/2^-$ (see data at bottom of figure 3 and further explanation of the curves below).

The solid lines in figure 3 represent the results of a CC calculation within the symmetric rotational model taking also into account Coulomb excitation and reorientation terms. The ECIS06 code was employed. The parameters of the optical potential used in the CC calculations

are given in table 2. They were fitted to the data shown in figure 3, using the OM1 parameters as an initial set. It was found that inelastic scattering data for the first three states of the rotational band may be well described if one assumes $\beta_\lambda R_V = 1.574$ fm and $\beta_2 = 0.64$. These values are consistent with results of previous studies [4].

Quadrupole moment $Q_{20}$ of the $^9$Be nucleus is known to be equal to +53 mb [23, 24] indicating a prolate deformation for the ground state. Previous studies (e.g. [4, 5]) have shown a quite large deformation parameter $\beta_2$ lying in the range 0.5 to 0.7. It provided rather good agreement with our data on elastic and inelastic (2.43 MeV and 6.76 MeV states) scattering. The obtained large $\beta_2$ value may be considered as the confirmation of the cluster structure of the low-lying states of $^9$Be. However it doesn't allow to give unambiguous preference to the one of the possible configurations, for example, $(\alpha + \alpha + \mathrm{n})$ or $(\alpha + {}^5\mathrm{He})$.

In figure 3, one may see a rather good agreement between the CC calculation and the experimental data (see solid line in the bottom part of figure 3) in the case of 11.28 MeV state. In order to improve the fits for this state, an additional hexadecapole term $\beta_4$ in the definition of the $^9$Be radius was added. The dash–double-dotted line in figure 3 demonstrates the result obtained with the same $\beta_2$ value and $\beta_4 = 0.27$, which agrees much better with the data. There is insignificant influence of the $\beta_4$ parameter on the cross sections for the $3/2^-$, $5/2^-$ and $7/2^-$ states. This may be evidence of the different structure of the $9/2^-$ state of the $^9$Be nucleus. It should be noted that data on inelastic scattering to the 11.28 MeV state were measured in the middle range of the angles, where the two theoretical predictions are rather comparable. Thus, in order to draw a firmer conclusion, additional measurements are required in a broader range of the scattering angles.

### 3.2. $^{10}$Be

If $^9$Be shows molecular cluster structure [3], then $^{10}$Be might be expected to show more sophisticated internal structure. Molecular structure of the $^{10}$Be nucleus is formed by two alpha particles and two neutrons. Such constitution attracts even more interest, since one neutron added to $^9$Be makes the $^{10}$Be nucleus tightly bound [15].

In this work we performed measurements of the angular distributions for the $^9$Be($^4$He,$^3$He)$^{10}$Be reaction, leading to different $^{10}$Be excited states. Angular distributions of the differential cross sections for the ground and low-lying excited states for $^{10}$Be are plotted in figure 4. Results of the present experiment are shown by solid symbols; data from [4] are presented by the open symbols. Solid lines are the results of the finite-range DWBA calculations with the DWUCK5 code [25]. This type of the calculation is available via the internet web page of the NRV project [26].

In order to perform the DWBA calculations the OM1 parameters for the entrance channel and the corresponding potential for the exit channel were chosen to calculate distorted waves (see table 1). OM parameters for the exit channel $^3$He + $^{10}$Be were chosen close to the potential recommended in [16]. According to table 1, Q-value for the $^9$Be($^4$He, $^3$He)$^{10}$Be reaction channel is negative with a large absolute value. This legitimizes a slight variation of the OM parameters for the exit channel (within 10%) for better agreement of the calculations with the data. In the analysis reported below we varied only the depths of the real and imaginary parts within indicated limits.

The single-particle wave functions in the entrance and exit channels were defined within the standard potential model [27, 28]. The interaction for $n + {}^3$He system was chosen of the Gaussian form

$$V(r) = -V_G \exp\left(-\frac{r^2}{R_G^2}\right),$$

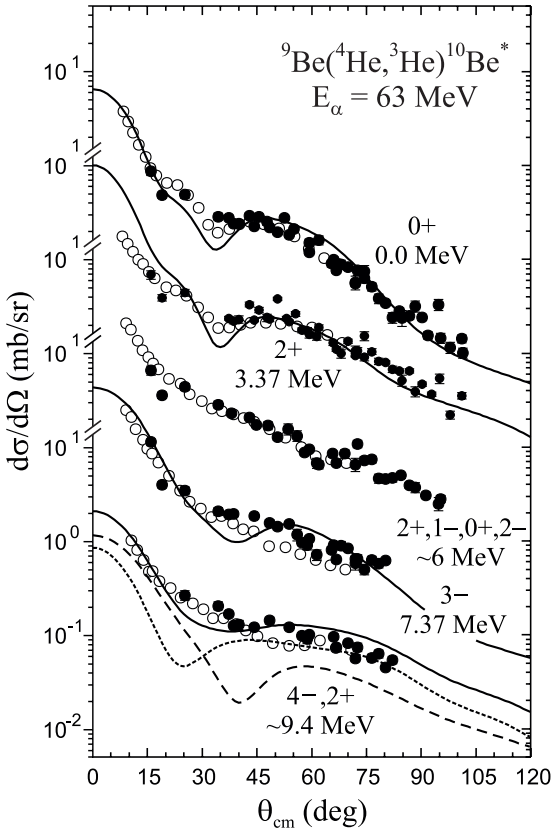


**Figure 4.** Angular distributions of the differential cross sections for the ground and low-lying excited states of $^{10}$Be in the reaction $^{9}$Be($^{4}$He,$^{3}$He)$^{10}$Be: the $0^{+}$ ground state of $^{10}$Be, the first $2^{+}$ state at 3.4 MeV, sum of cross sections for $2^{+}$, $1^{-}$, $0^{+}$ and $2^{-}$ levels between 5.9 and 6.3 MeV, the $3^{-}$ level at 7.3 MeV and sum of cross section for $4^{-}$ and $2^{+}$ levels at 9.3 MeV. Results of the present experiment are shown by solid symbols. Data from [4] are presented by open symbols. No DWBA curve is drawn through the differential cross sections for the $2^{+}$, $1^{-}$, $0^{+}$ and $2^{-}$ states, which are very close in the excitation energy and therefore could not be resolved. The curves are explained in the text.

where the radius $R_G = 2.452$ fm [28], while the potential depth $V_G$ is fitted to reproduce the correct value of the neutron binding energy $E_n = -20.58$ MeV in the $^{4}$He nucleus. The n + $^{9}$Be potential in the final state was defined as a real Woods–Saxon potential with radius $R_V = 1.26\ A_{Be}^{1/3}$ fm and diffuseness $a_V = 0.6$ fm. The potential depth $V_0$ defined in the same manner as the $V_G$ parameter. For states unbound to the neutron emission in $^{10}$Be, the single particle was assumed to be bound by 0.1 MeV, as it was suggested in [4].

The relative angular momentum of the neutron state in the projectile or target-like fragment was fixed by the total momentum $J$ and parity $\pi$ conservation laws. In particular, the ground state of the $^{10}$Be$(0^{+})$ = n$(1/2^{+})$ + $^{9}$Be$(3/2^{-})$ nucleus was considered as $1p_{3/2}$ neutron state, while the excited states of $^{10}$Be with negative parity were treated as $1d_{5/2}$ neutron states. All spectroscopic properties of the $^{10}$Be excited states are listed in table 3.

The DWBA differential cross section for the considered stripping reactions can be compared with experimental data in the following way [25]

**Table 3.** Spectroscopic information for the $^{9}$Be($\alpha$,$^{3}$He)$^{10}$Be and $^{9}$Be($\alpha$,$t$)$^{10}$B reactions, obtained from the DWBA analysis.

| $^{9}$Be($\alpha$,$^{3}$He)$^{10}$Be | | | | | $^{9}$Be($\alpha$,t)$^{10}$B | | | | |
|---|---|---|---|---|---|---|---|---|---|
| $E_x$,(MeV) | J$\pi$ | $l$ | $S_f$ [4] | $S_f$, present | $E_x$ (MeV) | J$\pi$ | $l$ | $S_f$ [4] | $S_f$, present |
| g.s. | $0^+$ | 1 | 1.58 | 1.65 | g.s. | $3^+$ | 1 | 0.89 | 0.59 |
| 3.368 | $2^+$ | 1 | 0.38 | 1.00 | 0.781 | $1^+$ | 1 | 1 | 1.0 |
| 5.958 | $2^+$ | 1 | $\leqslant$0.73 | $\leqslant$1.40 | 1.76 | $0^+$ | 1 | 1.58 | 1.38 |
| 5.960 | $1^-$ | 2 | $\leqslant$0.14 | $\leqslant$0.43 | 2.1 | $1^+$ | 1 | 0.52 | 0.30 |
| 6.179 | $0^+$ | 1 | – | – | 3.6 | $2^+$ | 1 | 0.28 | 0.23 |
| 6.263 | $2^-$ | 2 | 0.08 | $\leqslant$0.26 | 5.11 | $2^-$ | 2 | $\leqslant$0.27 | $\leqslant$0.16 |
| 7.371 | $3^-$ | 2 | 0.26 | 0.28 | 5.16 | $2^+$ | 1 | $\leqslant$1.85 | $\leqslant$0.75 |
| 7.542 | $2^+$ | 1 | – | – | 5.18 | $1^+$ | 1 | $\leqslant$3.14 | $\leqslant$1.0 |
| 9.27 | $(4^-)$ | 2 | $\leqslant$0.18 | 0.10 | 5.93 | $2^+$ | 1 | 0.48 | $\leqslant$0.95 |
| 9.56 | $2^+$ | 1 | – | 0.23 | 6.13 | $3^-$ | 2 | 0.24 | $\leqslant$0.19 |

$$\frac{\mathrm{d}\sigma_{\mathrm{exp}}}{\mathrm{d}\Omega} = S_i S_f \frac{(2J_f+1)}{(2J_i+1)}\sigma_{\mathrm{DW}}(q),$$

where $J_i = 3/2$ and $J_f$ are the angular momenta of the $^{9}$Be ground state and the final state populated in $^{10}$Be, respectively, $\sigma_{\mathrm{DW}}(\theta)$ is the output from DWUCK5, $S_i$ and $S_f$ are the projectile and target-like fragment spectroscopic factors, respectively. Figure 4 demonstrates how good are the obtained absolute values of the spectroscopic factors $S_f$, which were obtained from the comparison of the measured differential cross sections and DWUCK5 calculations for the different $^{10}$Be final states. The values of the spectroscopic factors are listed in table 3 together with $S_f$ values reported in [4].

It is seen that obtained cross sections agree well with data. The spectroscopic factors extracted from our analysis are very close to the ones listed in [4] (see table 3), except for the $^{10}$Be state at 3.368 MeV, where the spectroscopic values differ by more than a factor 2. The reason for this discrepancy is the following. The spectroscopic factor in our work was defined by adjusting the theoretical curve to the measured data in middle angle domain, while in [4] it was fitted to the forward experimental points near $\theta_{\mathrm{cm}} \approx 10^{\circ}$.

Because of the not-optimal value of the energy resolution, we were not able to separate the excited states nearby 6 MeV. Furthermore, the low statistics did not allow to observe the $2^+$ state at 7.54 MeV. The experimental cross sections corresponding to two overlapping states near 9.5 MeV were described as a sum of DWUCK5 outputs multiplied by the corresponding spectroscopic factors. Table 3 contains the $S_f$ values providing the best fit. The short and long-dashed lines in figure 4 show the contributions from the $2^+$ and $4^-$ states, respectively.

Note that in order to describe the data one needs much smaller radius of the real part of the optical potential for the exit channel ($r_V = 0.95$ fm) in comparison to the radius in the entrance channel ($r_V = 1.40$ fm). This could be interpreted as due to the compactness of the $^{10}$Be nucleus.

The nuclear charge radii of $^{7,9,10}$Be have been measured by high precision laser spectroscopy [21, 22]: the charge radius decreases form $^{7}$Be to $^{10}$Be. Comparing the Coulomb parameter $r_C$ with that of $^{9}$Be, we obtained a smaller value of $r_C$ for $^{10}$Be. In [21, 22], the decrease was explained as probably caused by the clusterization of $^{7}$Be into an $\alpha$ and triton clusters, whereas $^{9,10}$Be were considered to be $\alpha + \alpha +$ n and $\alpha + \alpha +$ n + n systems, respectively, and were more compact. The experimental trend was shown [15] to change beyond $^{10}$Be with an increase of the charge radius with atomic mass. Furthermore, the large

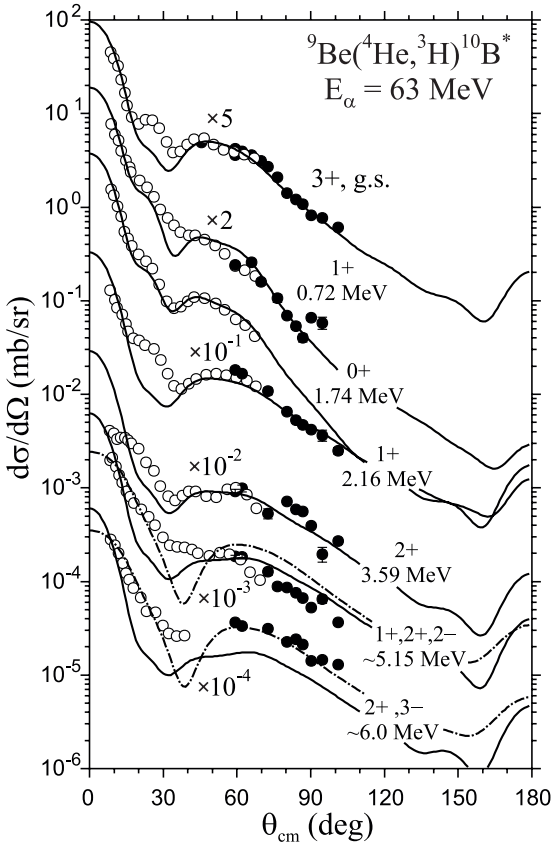


**Figure 5.** Angular distributions of the differential cross sections for the ground and low-lying excited states of $^{10}$B obtained in the reaction $^{9}$Be($\alpha$,$t$)$^{10}$B: the $3^{+}$ ground state of $^{10}$B, the first $1^{+}$ level at 0.72 MeV, the sum of the cross sections for the $0^{+}$ and $1^{+}$ levels at 1.7 and 2.1 MeV, respectively, from the present experiment superimposed over the cross section of the 2.16 MeV level from [4], the $2^{+}$ level at 3.6 MeV,the sum of the cross sections for the $2^{-}$, $2^{+}$ and $1^{+}$ levels at about 5.1 MeV, and the $3^{-}$ level at 6.1 MeV. Results of the present experiment are shown by solid symbols. Data from [4] are presented as open symbols.

experimental value of the charge radius for $^{12}$Be is consistent with a breakdown of the $N = 8$ shell closure.

The root-mean-square matter radii deduced by means of Glauber-model analysis with an optical limit approximation were reported in [29] and didn't show large difference in the values for $^{9}$Be and $^{10}$Be.

### *3.3.* $^{10}B$

Differential cross sections versus cm-angles for the ground and low-lying excited states of $^{10}$B are plotted in figure 5. Results of the present experiment are shown by solid symbols, and data from [4] are presented as open symbols. DWBA calculations [26] for the $^{9}$Be($\alpha$,$t$)$^{10}$B reaction were performed with the DWUCK5 code [25] with the fits to the differential cross sections for the ground and low-lying states given as thin solid lines in figure 5.

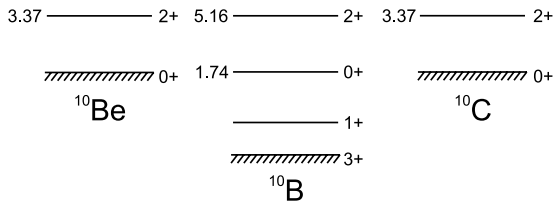


**Figure 6.** Level diagrams of low-lying states of $^{10}$Be, $^{10}$B and $^{10}$C, as members of the A = 10 multiplet. Values on the left side correspond to the excitation energies in MeV, while numbers on the right side are spins and parities of the corresponding states.

Figure 5 displays the observed angular distributions for the proton transfer reactions to the different $^{10}$B final states. One may note a very good agreement between the data obtained in [4] and our measurements. The theoretical results (solid and dash–dotted curves) fairly reproduce the data in case of well-defined final states. For the unresolved mixture of states at excitation energies of about 5.15 MeV and 6 MeV one may conclude that assuming negative parity states corresponding to $l = 2$ (shown by dash–dotted curves) provide better agreement with the data than assuming positive parity ones ($l = 1$, solid curves).

Spectroscopic factors $S_f$ for the different states populated in the reaction $^9$Be($\alpha$,$t$)$^{10}$B are listed on the right side in table 3. For the data corresponding to the mixture of a few levels, an upper limit of spectroscopic factor was obtained, describing the data by one component only. $S_f$ values are in good agreement with those reported in the literature.

### *3.4. Multiplet A = 10*

The structure of $^{10}$Be, $^{10}$B and $^{10}$C nuclei was usually considered as two $\alpha$-clusters in the presence of two extra nucleons. Level diagrams for the low-energy excited states for these nuclei are shown in figure 6. One may note that the $^{10}$B ground state is shifted down by 2 MeV approximately. It may be treated as a three cluster configuration $^{10}\mathrm{B} = \alpha + \mathrm{d} + \alpha$ where the pairing of proton and neutron results in formation of a deuteron cluster inside $^{10}$B. The $3^+$ spin of this state also supports this assumption. In the case of 1.74 MeV excited state, it might be considered as a state, where the deuteron cluster becomes unbound through excitation to proton–neutron $S = 0$ pair. Thus it becomes four clusters configuration $^{10}\mathrm{B}(0^+, 1.74\ \mathrm{MeV}) = \alpha + \mathrm{p} + \mathrm{n} + \alpha$ with uncorrelated proton and neutron ($S = 0$, $T = 1$). Two mirror ground states in $^{10}$Be and $^{10}$C in this case have to be of similar structure $\alpha + \mathrm{N} + \mathrm{N} + \alpha$. One of consequence of such an internal organization is the absence of the di-neutron component in the $^{10}$Be ground-state wave function.

The difference in the structures of the ground state and the 1.74 MeV state in $^{10}$B may also reveal itself in the difference of optical potentials for these exit channels. In figure 7 the corresponding experimental data are compared with the results of DWBA calculations performed following the same procedure as for the $^3$He + $^{10}$Be exit channel. The solid curves show theoretical cross sections obtained with the exit channel optical potential from table 3. This potential was chosen on the basis of OM potential compilation form [16] with additional adjustment of parameters to the present data since [16] contains recommended optical potentials for the lower energies. One may note a quite good agreement between DWBA calculation and data in the case of ground-state channel. Applying the same OMP for the transfer to the 1.74 MeV state one gets the noticeable overestimation in the cross section at large angles. We found that in order to improve the agreement in the last case it is necessary to use the following parameters: $V_0 = 85$ MeV, $r_V = 1.14$ fm and $W_0 = 8$ MeV. The corresponding

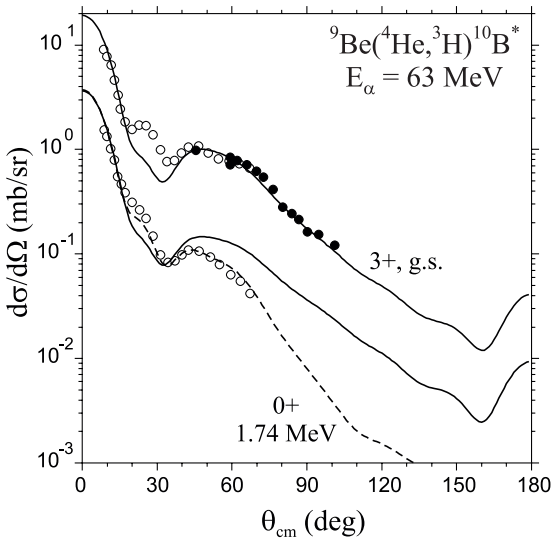


**Figure 7.** Differential cross sections for the reaction $^9$Be($^4$He,$t$)$^{10}$B leading to the ground and 1.74 MeV excited state of $^{10}$B nucleus. Solid symbols represent results of the present experiment, open ones are the data from [4]. Curves are the results of DWBA calculations (see text for explanations).

result is shown in figure 6 by the dashed curve and demonstrates excellent fit to the data. The obtained parameters turn out to be close to the OM potential for the $^3$He + $^{10}$Be(g.s.) channel (see table 2).

## 4. Conclusions

Angular distributions of the differential cross sections for the $^9$Be($\alpha$,$\alpha'$)$^9$Be$^*$, $^9$Be($\alpha$,$^3$He)$^{10}$Be and $^9$Be($^4$He,$t$)$^{10}$B reactions were measured. The observed states are most likely populated in one-step direct transfer reactions.

Experimental angular distributions for ground and a few low-lying states were described within the optical model (OM) and distorted-wave Born approximation frameworks. In the OM analysis and fits of the experimental data by coupled-channel (CC) calculations, it was found that the OM parameters ($V_0$, $W_0$, radii and diffuseness) were, in general, not sensitive to the cluster structures of the excited states. To study cluster structure, a complicated experiment is planned in which decay of excited states by cluster emission will be investigated. However, to distinguish break-up into $^4$He and $^5$He will be not be a trivial kinematical problem especially because $^5$He is unstable against decay to $n$ + $^4$He.

The values 9/2$^-$ were assigned to the spin and parity of the 11.28 MeV state in $^9$Be. The obtained large $\beta_2$ value may be considered as confirmation of the cluster structure of the low-lying states of $^9$Be. However, it does not allow to give unambiguous preference to one of the possible configurations $\alpha + \alpha$ + n or $\alpha$ + $^5$He. In order to improve the agreement between the theoretical prediction and the experimental data, related to this 9/2$^-$ state, an additional hexadecapole term $\beta_4$ in the definition of the $^9$Be radius had to be introduced.

With respect to $^{10}$Be, it was found that in order to describe the data one needs a much smaller radius of the real part of the optical potential for the exit channel ($r_V = 0.95$ fm) in comparison to the radius in the entrance channel ($r_V = 1.40$ fm). This could be interpreted as evidence for the compactness of the $^{10}$Be nucleus.

The comparison of the angular distributions of the differential cross sections for the isobaric analog states of $^{10}$Be and $^{10}$B was done. The structure of $^{10}$Be, $^{10}$B and $^{10}$C nuclei was usually considered as two $\alpha$-clusters in the presence of two extra nucleons. One may see that the $^{10}$B ground state could be treated as a three cluster configuration $^{10}\mathrm{B} = \alpha + \mathrm{d} + \alpha$, where the pairing of proton and neutron results in formation of a deuteron cluster inside $^{10}$B. In the case of the 1.74 MeV excited state, it might be considered as a state where the deuteron cluster becomes unbound. Thus, it becomes a four-body configuration $^{10}\mathrm{B}(0^+, 1.74\ \mathrm{MeV}) = \alpha + \mathrm{p} + \mathrm{n} + \alpha$, i.e. two $\alpha$-clusters with an uncorrelated proton and neutron pair ($S = 0$, $T = 0$).

Spectroscopic factors for the ground and excited states of $^{10}$B and $^{10}$Be were deduced. We found pretty good agreement between our results and the previous data.

## Acknowledgments

We would like to thank the JYFL Accelerator Laboratory for giving us the opportunity to perform this study and the cyclotron staff for the excellent beam quality. This work was supported in part by the Russian Foundation for Basic Research (project numbers: 13-02-00533 and 13-07-00714), by grants to JINR (Dubna) of the Czech and Polish Republics, and by mobility grant from the Academy of Finland.

## References

[1] Penionzhkevich Y E *et al* 2009 Complete and incomplete fusion of $^6$Li ions with Bi and Pt *J. Phys. G: Nucl. Part. Phys.* **36** 025104
[2] Skobelev N K, Demekhina N A, Kalpakchieva R, Kulko A A, Lukyanov S M, Muzychka Y A, Penionzhkevich Y E and Chuvilskaya T V 2009 The excitation functions of complete and incomplete fusion reactions of $^6$Li with Pt nuclei *Phys. Part. Nucl. Lett.* **6** 208–15
[3] von Oertzen W 2009 *Proc. Int. Symp. on Exotic Nuclei* ed Y E Penionzhkevich and S M Lukyanov (New York: AIP) p 161
[4] Harakeh M N, Van Popta J, Saha A and Siemssen R H 1980 Strong coupled-channels effects in the $^9$Be($\alpha$, t)$^{10}$B reaction *Nucl. Phys.* A **344** 15–40
[5] Roy S, Chatterjee J M, Majumdar H, Datta S K, Banerjee S R and Chintalapudi S N 1995 Coupled channel folding model description of $\alpha$ scattering from $^9$Be *Phys. Rev.* C **52** 1524–31
[6] Rudchik A T, Momotyuk O A, Ziman V A, Budzanowski A, Szczurek A, Skwirczyska I, Kliczewski S and Siudak R 2000 Energy dependence of the nucleus–nucleus interaction in the $^9$Be + $^{12}$C system and the $^9$Be reorientation *Nucl. Phys.* A **662** 44–62
[7] Keeley N, Kemper K W and Rusek K 2001 $^5$He + $\alpha$ cluster model of $^9$Be breakup *Phys. Rev.* C **64** 031602
[8] Fortune H T and Sherr R 2013 Continuum three-body decays of $^9$Be($5/2^-$) *Phys. Rev.* C **87** 014306
[9] Charity R J, Wiser T D, Mercurio K, Shane R, Sobotka L G, Wuosmaa A H, Banu A, Trache L and Tribble R E 2009 Continuum spectroscopy with a $^{10}$C beam: cluster structure and three-body decay *Phys. Rev.* C **80** 024306
[10] Tilley D R, Kelley J H, Godwin J L, Millener D J, Purcell J E, Sheu C G and Weller H R 2004 Energy levels of light nuclei *Nucl. Phys.* A **745** 155–362
[11] Bohlen H G, Dorsch T, Kokalova T, von Oertzen W, Schulz C and Wheldon C 2007 Structure of $^{10}$Be from the $^{12}$C($^{12}$C,$^{14}$O)$^{10}$Be reaction *Phys. Rev.* C **75** 054604
[12] Miura K *et al* 1992 The $^9$Be(d,n)$^{10}$B reaction at 25 MeV *Nucl. Phys.* A **539** 441–50
[13] Zagrebaev V I, Denikin A S and Alekseev A P 2000 Optical model of elastic scattering (http://nrv.jinr.ru/nrv/) Nuclear Reaction Video Project
[14] Raynal J 1972 Computing as a language of physics *Proc. ICTP Int. Seminar Course (Trieste, Italy, 1971)* (Vienna: IAEA) p 281
[15] Raynal J 2006 Computer code ECIS 06 unpublished
[16] Perey C M and Perey F G 1974 Compilation of phenomenological optical-model parameters 1969–1972 *At. Data Nucl. Data Tables* **13** 293–337

[17] Brown T A D *et al* 2007 Decay studies for states in $^{9}$Be up to 11 MeV: insights into the n + $^{8}$Be and $\alpha$ + $^{5}$He cluster structure *Phys. Rev.* C **76** 054605
[18] Koike Y 2008 $^{9}$Be: a gateway nucleus into heavier nuclei? arXiv:nucl-th/0201075
[19] Ajzenberg-Selove F 1988 Energy levels of light nuclei A = 510 *Nucl. Phys.* A **490** 1–225
[20] Votava H J, Clegg T B, Ludwig E J and Thompson W J 1973 Proton scattering from $^{9}$Be between 6 and 30 MeV and the structure of $^{9}$Be *Nucl. Phys.* A **204** 529–51
[21] Nörtershäuser W *et al* 2009 Nuclear charge radii of $^{7,9,10}$Be and the one-neutron halo nucleus $^{11}$Be *Phys. Rev. Lett.* **102** 062503
[22] Krieger A *et al* 2012 Nuclear charge radius of $^{12}$Be *Phys. Rev. Lett.* **108** 142501
[23] Blachman A G and Lurio A 1967 Hyperfine structure of the metastable $(1s^2 2s2p)^3$p states of $_4$Be$^9$ and the nuclear electric quadrupole moment *Phys. Rev.* **153** 164–76
[24] Stone N J 2005 Table of nuclear magnetic dipole and electric quadrupole moments *At. Data Nucl. Data Tables* **90** 75–176
[25] Kunz P Computer code DWUCK5 (http://spot.colorado.edu/kunz/DWBA.html)
[26] Zagrebaev V I, Denikin A S and Alekseev A P 2009 DWBA for nucleon transfer reactions (http://nrv.jinr.ru/nrv/webnrv/transfer/) Nuclear Reaction Video Project
[27] Dubovichenko S B and Dzhazairov-Kakhmanov A V 1997 Electromagnetic effects in light nuclei within cluster potential model *Phys. Part. Nucl.* **28** 1529–94
[28] Denikin A S, Zagrebaev V I and Descouvemont P 2009 Generalized optical potential for weakly bound nuclei: two-cluster projectiles *Phys. Rev.* C **79** 024605
[29] Ozawa A, Suzuki T and Tanihata I 2001 Nuclear size and related topics *Nucl. Phys.* A **693** 32–62